

GENERATIVE MAX-MAHALANOBIS CLASSIFIERS FOR IMAGE CLASSIFICATION, GENERATION AND MORE

Xiulong Yang, Hui Ye, Yang Ye, Xiang Li & Shihao Ji

Department of Computer Science

Georgia State University

{xyang22, hye2, yyel10, xli62, sji}@gsu.edu

ABSTRACT

Joint Energy-based Model (JEM) of Grathwohl et al. (2020a) shows that a standard softmax classifier can be reinterpreted as an energy-based model (EBM) for the joint distribution $p(\mathbf{x}, y)$; the resulting model can be optimized to improve calibration, robustness and out-of-distribution detection, while generating samples rivaling the quality of recent GAN-based approaches. However, the softmax classifier that JEM exploits is inherently discriminative and its latent feature space is not well formulated as probabilistic distributions, which may hinder its potential for image generation and incur training instability. We hypothesize that generative classifiers, such as Linear Discriminant Analysis (LDA), might be more suitable for image generation since generative classifiers model the data generation process explicitly. This paper therefore investigates an LDA classifier for image classification and generation. In particular, the Max-Mahalanobis Classifier (MMC) Pang et al. (2020), a special case of LDA, fits our goal very well. We show that our Generative MMC (GMMC) can be trained discriminatively, generatively or jointly for image classification and generation. Extensive experiments on multiple datasets show that GMMC achieves state-of-the-art discriminative and generative performances, while outperforming JEM in calibration, adversarial robustness and out-of-distribution detection by a significant margin. Our source code is available at <https://github.com/sndnyang/GMMC>.

1 INTRODUCTION

Over the past few years, deep neural networks (DNNs) have achieved state-of-the-art performance on a wide range of learning tasks, such as image classification, object detection, segmentation and image captioning Krizhevsky & Hinton (2009); He et al. (2016). All of these breakthroughs, however, are achieved in the framework of discriminative models, which are known to be exposed to several critical issues, such as adversarial examples Goodfellow et al. (2015), calibration of uncertainty Guo et al. (2017) and out-of-distribution detection Hendrycks & Gimpel (2016). Prior works have shown that generative training is beneficial to these models and can alleviate some of these issues at certain levels Chapelle et al. (2009); Dempster et al. (1977). Yet, most recent research on generative models focus primarily on qualitative sample quality Brock et al. (2019); Santurkar et al. (2019); Vahdat & Kautz (2020), and the discriminative performances of state-of-the-art generative models are still far behind discriminative ones Behrmann et al. (2018); Chen et al. (2019); Du & Mordatch (2019).

Recently, there is a flurry of interest in closing the performance gap between generative models and discriminative models Du & Mordatch (2019); Grathwohl et al. (2020a); Gao et al. (2020); Ardizzone et al. (2020). Among them, IGEBM Du & Mordatch (2019) and JEM Grathwohl et al. (2020a) are the two most representative ones, which reinterpret CNN classifiers as the energy-based models (EBMs) for image generation. Since the CNN classifier is the only trained model, which has a high compositionality, it is possible that a single trained CNN model may encompass the generative capabilities into the discriminative model without sacrificing its discriminative power. Their works realize the potential of EBMs in hybrid modeling and achieve improved performances on discriminative and generative tasks. Specifically, JEM Grathwohl et al. (2020a) reinterprets the

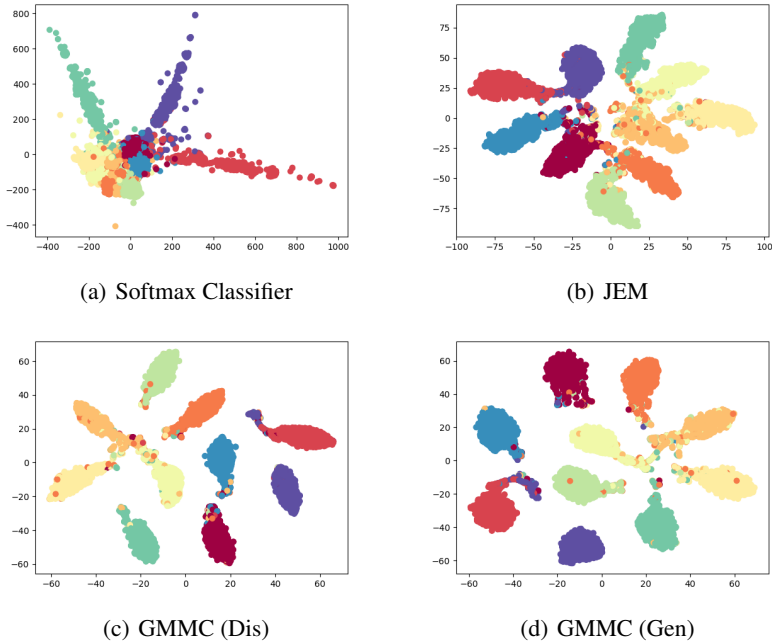


Figure 1: t-SNE visualization of the latent feature spaces learned by different models trained on CIFAR10.

standard softmax classifier as an EBM and achieves impressive performances in image classification and generation simultaneously, and ignites a series of follow-up works Zhao et al. (2020); Grathwohl et al. (2020b); Gao et al. (2020). However, the softmax classifier that JEM exploits is inherently discriminative, which may hinder its potential in image generation. To investigate this, we visualize the latent feature spaces learnt by a standard softmax classifier and by JEM through t-SNE Maaten & Hinton (2008) in Figs. 1(a) and 1(b), respectively. Apparently, the feature space of the softmax classifier has been improved significantly by JEM as manifested by higher inter-class separability and intra-class compactness. However, JEM’s latent space is not well formulated as probabilistic distributions, which may limit its generative performance and incur training instability as observed in Grathwohl et al. (2020a). We hypothesize that generative classifiers (e.g., LDA) might be more suitable for image classification and generation. This is because generative classifiers model the data generation process explicitly with probabilistic distributions, such as mixture of Gaussians, which aligns well with the generative process of image synthesis. Therefore, in this paper we investigate an LDA classifier for image classification and generation. In particular, the Max-Mahalanobis Classifier (MMC) Pang et al. (2020), a special case of LDA, fits our goal very well since MMC formulates the latent feature space explicitly as the Max-Mahalanobis distribution Pang et al. (2018). Distinct to Pang et al. (2020), we show that MMC can be trained discriminatively, generatively or jointly as an EBM. We term our algorithm Generative MMC (GMMC) given that it is a hybrid model for image classification and generation, while the original MMC Pang et al. (2020) is only for classification.

As a comparison, Figs. 1(c) and 1(d) illustrate the latent feature spaces of GMMC optimized with discriminative training and generative training (to be discussed in Sec. 3), respectively. It can be observed that the latent feature spaces of GMMC are improved even further over that of JEM’s with higher inter-class separability and intra-class compactness. Furthermore, the explicit generative modeling of GMMC also leads to many auxiliary benefits, such as adversarial robustness, calibration of uncertainty and out-of-distribution detection, as to be demonstrated in our experiments. Our main contributions can be summarized as follows:

1. We introduce GMMC a hybrid model for image classification and generation. As an alternative to the softmax classifier utilized in JEM, GMMC has a well-formulated latent feature distribution, which fits well with the generative process of image synthesis.

2. We show that GMMC can be trained discriminatively, generatively or jointly with reduced complexity and improved stability as compared to JEM.
3. Our model matches or outperforms prior state-of-the-art hybrid models on multiple discriminative and generative tasks, including image classification, image synthesis, calibration of uncertainty, out-of-distribution detection and adversarial robustness.

2 BACKGROUND AND RELATED WORK

2.1 ENERGY-BASED MODELS

Energy-based models (EBMs) LeCun et al. (2006) define an energy function that assigns low energy values to samples drawn from data distribution and high values otherwise, such that any probability density $p_{\theta}(\mathbf{x})$ can be expressed via a Boltzmann distribution as

$$p_{\theta}(\mathbf{x}) = \exp(-E_{\theta}(\mathbf{x})) / Z(\theta), \quad (1)$$

where $E_{\theta}(\mathbf{x})$ is an energy function that maps each input $\mathbf{x} \in \mathbb{R}^D$ to a scalar, and $Z(\theta)$ is the normalizing constant (also known as the partition function) such that $p_{\theta}(\mathbf{x})$ is a valid density function.

The key challenge of training EBMs lies in estimating the partition function $Z(\theta)$, which is notoriously intractable. The standard maximum likelihood estimation of parameters θ is not straightforward, and a number of sampling-based approaches have been proposed to approximate it effectively. Specifically, the gradient of the log-likelihood of a single sample \mathbf{x} w.r.t. θ can be expressed as

$$\frac{\partial \log p_{\theta}(\mathbf{x})}{\partial \theta} = \mathbb{E}_{p_{\theta}(\mathbf{x}')} \frac{\partial E_{\theta}(\mathbf{x}')}{\partial \theta} - \frac{\partial E_{\theta}(\mathbf{x})}{\partial \theta}, \quad (2)$$

where the expectation is over data distribution $p_{\theta}(\mathbf{x}')$, sampling from which is challenging due to the intractable $Z(\theta)$. Therefore, MCMC and Gibbs sampling Hinton (2002) have been proposed previously to estimate the expectation efficiently. To speed up the mixing for effective sampling, recently Stochastic Gradient Langevin Dynamics (SGLD) Welling & Teh (2011) has been used to train EBMs by exploiting the gradient information Nijkamp et al. (2019b); Du & Mordatch (2019); Grathwohl et al. (2020a). Specifically, to sample from $p_{\theta}(\mathbf{x})$, SGLD follows

$$\begin{aligned} x_0 &\sim p_0(\mathbf{x}), \\ x_{i+1} &= x_i - \frac{\alpha}{2} \frac{\partial E_{\theta}(x_i)}{\partial x_i} + \alpha \epsilon, \quad \epsilon \sim \mathcal{N}(0, 1), \end{aligned} \quad (3)$$

where $p_0(\mathbf{x})$ is typically a Uniform distribution over $[-1, 1]$, whose samples are refined via noisy gradient decent with step-size α , which should be decayed following a polynomial schedule.

Besides JEM Grathwohl et al. (2020a) that we discussed in the introduction, Xie et al. (2016) is an earlier work that derives a generative CNN model from the commonly used discriminative CNN by treating it as an EBM. The authors factorize the loss function $\log p(\mathbf{x}|y)$ as an EBM, which is similar to ours. Following-up works, such as Nijkamp et al. (2019a); Du & Mordatch (2019), scale the training of EBMs to high-dimensional data using SGLD. However, all of these previous methods define $p(\mathbf{x}|y)$ as a separate EBM with a distinct, intractable normalizing constant. Therefore, their models cannot be used to compute $p(y|\mathbf{x})$ or $p(\mathbf{x})$ efficiently, while our GMMC defines $p(\mathbf{x}|y)$ explicitly as a Gaussian distribution, which simplifies the maximum likelihood estimation significantly and achieves superior performances in many discriminative and generative tasks.

2.2 ALTERNATIVES TO THE SOFTMAX CLASSIFIER

Softmax classifier has been widely used in state-of-the-art models for discriminative tasks due to its simplicity and efficiency. However, softmax classifier is known particularly vulnerable to adversarial attacks because the latent feature space induced by softmax classifier is typically not well separated (as shown in Fig. 1(a)). Some recent works propose to use generative classifiers to better formulate the latent space distributions in order to improve its robustness to adversarial attacks. For example, Wan et al. (2018) proposes to model the latent feature space as mixture of Gaussians and encourages stronger intra-class compactness and larger inter-class separability by introducing large margins between classes. Different from Wan et al. (2018), Pang et al. (2018) pre-designs centroids

based on the max-Mahalanobis distribution (MMD), instead of learning them from data. The authors prove that if the latent feature space distributes as a MMD, the LDA classifier will have the best robustness to adversarial examples. Taking advantage of the benefits of MMD, Pang et al. (2020) further proposes a max-Mahalanobis center regression loss, which induces much denser feature regions and improves the robustness of trained models. Compared with softmax classifier, all these works can generate better latent feature spaces to improve the robustness of models for the task of classification. Our GMMC is built on the basic framework of MMC, but we reinterpret MMC as an EBM for image classification and generation. Moreover, we show that the generative training of MMC can further improve calibration, adversarial robustness and out-of-distribution detection.

3 METHODOLOGY

We assume a Linear Discriminant Analysis (LDA) classifier is defined as: $\phi(\mathbf{x})$, $\boldsymbol{\mu} = \{\boldsymbol{\mu}_y, y = 1, 2, \dots, C\}$ and $\boldsymbol{\pi} = \{\pi_y = \frac{1}{C}, y = 1, 2, \dots, C\}$ for C -class classification, where $\phi(\mathbf{x}) \in \mathbb{R}^d$ is the feature representation of \mathbf{x} extracted by a CNN, parameterized by ϕ , and $\boldsymbol{\mu}_y \in \mathbb{R}^d$ is the mean of a Gaussians distribution with a diagonal covariance matrix $\gamma^2 \mathbf{I}$, i.e., $\mathcal{N}(\boldsymbol{\mu}_y, \gamma^2 \mathbf{I})$. Therefore, we can parameterize LDA by $\boldsymbol{\theta} = \{\phi, \boldsymbol{\mu}\}^1$. Instead of using this regular LDA classifier, in this paper the max-Mahalanobis classifier (MMC) Pang et al. (2020), a special case of LDA, is considered. Different from the LDA modeling above, in MMC $\boldsymbol{\mu} = \{\boldsymbol{\mu}_y, y = 1, 2, \dots, C\}$ is pre-designed to induce compact feature representations for model robustness. We found that the MMC modeling fits our goal better than the regular LDA classifier due to its improved training stability and boosted adversarial robustness. Therefore, in the following we focus on the MMC modeling for image classification and generation. As such, the learnable parameters of MMC reduce to $\boldsymbol{\theta} = \{\phi\}$, and the algorithm to calculate pre-designed $\boldsymbol{\mu}$ can be found in Algorithm 2 in the Appendix. An overview of the training and test of our GMMC algorithm is illustrated in Fig. 2, with the details discussed below.

Instead of maximizing $p_{\boldsymbol{\theta}}(y|\mathbf{x})$ as in standard softmax classifier, following JEM Grathwohl et al. (2020a) we maximize the joint distribution $p_{\boldsymbol{\theta}}(\mathbf{x}, y)$, which is defined as a mixture of Gaussians distribution in MMC. To optimize $\log p_{\boldsymbol{\theta}}(\mathbf{x}, y)$, we can consider three approaches.

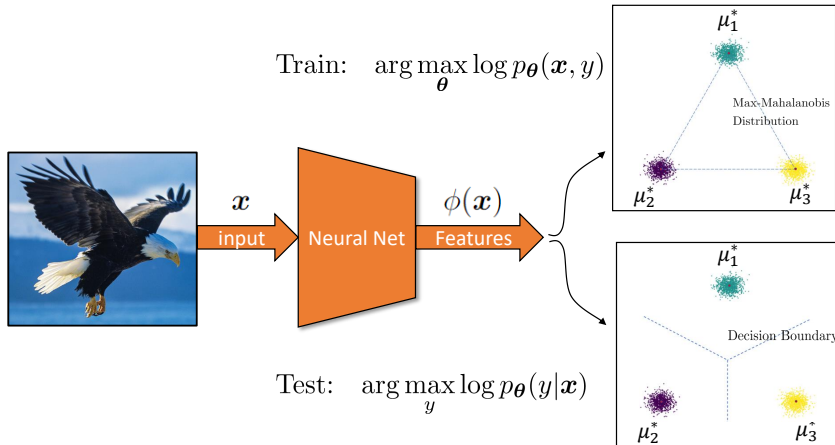


Figure 2: Overview of GMMC for training and test, where the model can be trained discriminatively, generatively or jointly. $\{\mu_1^*, \mu_2^*, \dots, \mu_C^*\}$ are pre-designed according to MMD Pang et al. (2018). Only $\boldsymbol{\theta} = \{\phi\}$ is learned from data.

¹We can treat γ as a tunable hyperparameter or we can estimate it by post-processing. In this work, we take the latter approach as discussed in Sec. 3.1.

3.1 APPROACH 1: DISCRIMINATIVE TRAINING

According to the MMC modeling above, the log of the joint distribution can be simplified as

$$\begin{aligned}\log p_{\theta}(\mathbf{x}, y) &= \log p(y) + \log p_{\theta}(\mathbf{x}|y) \\ &= -\frac{1}{2\gamma^2} \|\phi(\mathbf{x}) - \boldsymbol{\mu}_y\|_2^2 + \text{constant} \\ &= -E_{\theta}(\mathbf{x}, y) + \text{constant},\end{aligned}\tag{4}$$

where we define $E_{\theta}(\mathbf{x}, y) = \frac{1}{2\gamma^2} \|\phi(\mathbf{x}) - \boldsymbol{\mu}_y\|_2^2$. To optimize the parameters θ , we can simply compute gradient of Eq. 4 w.r.t. θ , and update the parameters by stochastic gradient descent (SGD) Robbins & Monro (1951). Note that γ is a constant in Eq. 4, its effect can be absorbed into the learning rate when optimizing Eq. 4 via SGD. After convergence, we can estimate $\gamma^2 = \frac{1}{d} \left(\frac{1}{N} \sum_{i=1}^N \|\phi(\mathbf{x}_i) - \boldsymbol{\mu}_i\|_2^2 \right)$ from training set by using optimized ϕ and pre-designed $\boldsymbol{\mu}$.

Note that Eq. 4 boils down to the same objective that MMC Pang et al. (2020) proposes, i.e. the center regression loss. While MMC reaches to this objective from the perspective of inducing compact feature representations for model robustness, we arrive at this objective by simply following the principle of maximum likelihood of joint density $p_{\theta}(\mathbf{x}, y)$.

3.2 APPROACH 2: GENERATIVE TRAINING

Alternatively, $p_{\theta}(\mathbf{x}, y)$ can be considered as an EBM of (\mathbf{x}, y)

$$\begin{aligned}p_{\theta}(\mathbf{x}, y) &= p(y)p_{\theta}(\mathbf{x}|y) \\ &= \frac{1}{C} (2\pi\gamma^2)^{-d/2} \exp\left(-\frac{1}{2\gamma^2} \|\phi(\mathbf{x}) - \boldsymbol{\mu}_y\|_2^2\right) \\ &= \frac{\exp\left(-\frac{1}{2\gamma^2} \|\phi(\mathbf{x}) - \boldsymbol{\mu}_y\|_2^2\right)}{Z}.\end{aligned}\tag{5}$$

Note that different from standard EBM, here Z is not a function of θ due to the Gaussian modeling of MMC. From Eq. 5, we can see that $E_{\theta}(\mathbf{x}, y) = \frac{1}{2\gamma^2} \|\phi(\mathbf{x}) - \boldsymbol{\mu}_y\|_2^2$ is essentially an energy function of (\mathbf{x}, y) .

To optimize Eq. 5, we can compute its gradient w.r.t. θ by treating it as an EBM (see Eq. 2)

$$\frac{\partial \log p_{\theta}(\mathbf{x}, y)}{\partial \theta} = \beta \mathbb{E}_{p_{\theta}(\mathbf{x}', y')} \frac{\partial E_{\theta}(\mathbf{x}', y')}{\partial \theta} - \frac{\partial E_{\theta}(\mathbf{x}, y)}{\partial \theta},\tag{6}$$

where β is a hyperparameter that balances the contributions from the two terms. It can be proved readily that Eq. 6 holds for any $\beta \in \mathbb{R}$ since the first term is 0 in expectation (again due to the Gaussian modeling of MMC). Therefore, Eq. 6 is exact, not an approximation. However, in practice since we estimate the expectation with Monte Carlo samples, different β has a significant impact to the performance. From our experiments, we find that $\beta = 0.5$ works very well in all our cases. Similar to the discriminative training above, γ is a constant in the energy function, so its effect can be absorbed into the learning rate when optimizing Eq. 6 via SGD.

The tricky part is how to generate samples $(\mathbf{x}', y') \sim p_{\theta}(\mathbf{x}', y')$ to estimate the first term of Eq. 6. We can follow the mixture of Gaussians assumption of MMC, i.e., $p_{\theta}(\mathbf{x}', y') = p(y')p_{\theta}(\mathbf{x}'|y')$: (1) sample $y' \sim p(y') = \frac{1}{C}$, and then (2) sample $\mathbf{x}' \sim p_{\theta}(\mathbf{x}'|y') = \mathcal{N}(\boldsymbol{\mu}_{y'}, \gamma^2 \mathbf{I})$. To sample \mathbf{x}' , again we can consider two choices.

(1) Staged Sampling We can first sample $\mathbf{z}_{x'} \sim \mathcal{N}(\boldsymbol{\mu}_{y'}, \gamma^2 \mathbf{I})$, and then find a \mathbf{x}' to minimize $E_{\theta}(\mathbf{x}') = \frac{1}{2\gamma^2} \|\phi(\mathbf{x}') - \mathbf{z}_{x'}\|_2^2$. This can be achieved by

$$\mathbf{x}'_0 \sim p_0(\mathbf{x}'), \quad \mathbf{x}'_{t+1} = \mathbf{x}'_t - \alpha \frac{\partial E_{\theta}(\mathbf{x}'_t)}{\partial \mathbf{x}'_t},\tag{7}$$

where $p_0(\mathbf{x})$ is typically a Uniform distribution over $[-1, 1]$. Note that this is similar to SGLD (see Eq. 3) but without a noisy term. Thus, the training could be more stable. In addition, the function $E_{\theta}(\mathbf{x}') = \frac{1}{2\gamma^2} \|\phi(\mathbf{x}') - \mathbf{z}_{x'}\|_2^2$ is just an L_2 regression loss (not an LogSumExp function as used in Grathwohl et al. (2020a)). This may lead to additional numerical stability.

Algorithm 1 Generative training of GMMC: Given network f_θ , step-size α , replay buffer B , number of steps τ , reinitialization frequency ρ , and number of classes C

```

1: while not converged do
2:   Sample  $\mathbf{x}$  and  $y$  from dataset  $\mathcal{D}$ 
3:   Sample  $(\mathbf{x}'_0, y') \sim B$  with probability  $1 - \rho$ , else  $\mathbf{x}'_0 \sim \mathcal{U}(-1, 1), y' \sim p(y') = \frac{1}{C}$ 
4:   Sample  $\mathbf{z}_{\mathbf{x}'_0} \sim \mathcal{N}(\boldsymbol{\mu}_{y'}, \gamma^2 \mathbf{I})$  if staged sampling
5:   for  $t \in [1, 2, \dots, \tau]$  do
6:     Sample  $\mathbf{z} \sim \mathcal{N}(\mathbf{0}, \mathbf{I}), \mathbf{z}_{\mathbf{x}'_t} = \boldsymbol{\mu}_{y'} + \gamma^2 \mathbf{z}$  if noise injected sampling
7:      $\mathbf{x}'_t = \mathbf{x}'_{t-1} - \alpha \frac{\partial E_\theta(\mathbf{x}'_{t-1})}{\partial \mathbf{x}'_{t-1}}$  (Eq. 7)
8:   end for
9:   Calculate gradient with Eq. 6 from  $(\mathbf{x}, y)$  and  $(\mathbf{x}'_\tau, y')$  for model update
10:  Add / replace updated  $(\mathbf{x}'_\tau, y')$  back to  $B$ 
11: end while
    
```

(2) Noise Injected Sampling We can first sample $\mathbf{z} \sim \mathcal{N}(\mathbf{0}, \mathbf{I})$, then by the reparameterization trick we have $\mathbf{z}_{\mathbf{x}'_t} = \gamma \mathbf{z} + \boldsymbol{\mu}_{y'}$. Finally, we can find a \mathbf{x}' to minimize

$$\begin{aligned}
 E_\theta(\mathbf{x}') &= \frac{1}{2\gamma^2} \|\phi(\mathbf{x}') - \mathbf{z}_{\mathbf{x}'}\|_2^2 = \frac{1}{2\gamma^2} \|\phi(\mathbf{x}') - \boldsymbol{\mu}_{y'} - \gamma \mathbf{z}\|_2^2 \\
 &= \frac{1}{2\gamma^2} \|\phi(\mathbf{x}') - \boldsymbol{\mu}_{y'}\|_2^2 + \frac{1}{2\gamma^2} \|\mathbf{z}\|_2^2 - \frac{1}{\gamma} \langle \phi(\mathbf{x}') - \boldsymbol{\mu}_{y'}, \gamma \mathbf{z} \rangle \\
 &= E_\theta(\mathbf{x}', y') + \frac{1}{2\gamma^2} \|\mathbf{z}\|_2^2 - \frac{1}{\gamma} \langle \phi(\mathbf{x}') - \boldsymbol{\mu}_{y'}, \mathbf{z} \rangle.
 \end{aligned} \tag{8}$$

This can be achieved by

$$\begin{aligned}
 \mathbf{x}'_0 &\sim p_0(\mathbf{x}'), \\
 \mathbf{x}'_{t+1} &= \mathbf{x}'_t - \alpha \frac{\partial E_\theta(\mathbf{x}'_t)}{\partial \mathbf{x}'_t} \\
 &= \mathbf{x}'_t - \alpha \frac{\partial E_\theta(\mathbf{x}'_t, y')}{\partial \mathbf{x}'_t} + \alpha \frac{1}{\gamma} \langle \frac{\partial \phi(\mathbf{x}'_t)}{\partial \mathbf{x}'_t}, \mathbf{z} \rangle,
 \end{aligned} \tag{9}$$

where we sample a different \mathbf{z} at each iteration. As a result, Eq. 9 is an analogy of SGLD (see Eq. 3). The difference is that instead of using an unit Gaussian noise, $\epsilon \sim \mathcal{N}(0, 1)$, as in SGLD, a gradient-modulated noise (the 3rd term) is applied.

Algorithm 1 provides the pseudo-code of the generative training of GMMC, which follows a similar design of JEM Grathwohl et al. (2020a) and IGEBM Du & Mordatch (2019). For brevity, only one real sample $(\mathbf{x}, y) \sim \mathcal{D}$ and one generated sample $(\mathbf{x}', y') \sim p_\theta(\mathbf{x}', y')$ are used to optimize the parameter θ . It is straightforward to generalize the pseudo-code above to a mini-batch training, which is used in our experiments. Compared to JEM, GMMC needs no additional calculation of $p_\theta(y|\mathbf{x})$ and thus has reduced computational complexity.

3.3 APPROACH 3: JOINT TRAINING

Comparing Eq. 4 and Eq. 6, we note that the gradient of Eq. 4 is just the second term of Eq. 6. Hence, we can use (approach 1) discriminative training to pretrain θ , and then finetune θ by (approach 2) generative training, and this joint strategy would be stable since the first term of Eq. 6 is 0 in expectation. Similar joint training strategy could be applied to train JEM. However, from our experiments we note that this joint training of JEM is extremely unstable likely due to dramatic differences in the learned parameters of two different approaches for JEM. We will demonstrate this when we present results.

3.4 GMMC FOR INFERENCE

After training with one of the three approaches discussed above, we get the optimized GMMC parameters $\theta = \{\phi\}$, the pre-designed $\boldsymbol{\mu}$ and the estimated $\gamma^2 = \frac{1}{d} \left(\frac{1}{N} \sum_{i=1}^N \|\phi(\mathbf{x}_i) - \boldsymbol{\mu}_i\|_2^2 \right)$

from training set. We can then calculate class probabilities for classification

$$p_{\theta}(y|\mathbf{x}) = \frac{\exp(-\frac{1}{2\gamma^2}\|\phi(\mathbf{x}) - \boldsymbol{\mu}_y\|_2^2)}{\sum_{y'} \exp(-\frac{1}{2\gamma^2}\|\phi(\mathbf{x}) - \boldsymbol{\mu}_{y'}\|_2^2)}. \quad (10)$$

4 EXPERIMENTS

We evaluate the performance of GMMC on multiple discriminative and generative tasks, including image classification, image generation, calibration of uncertainty, out-of-distribution detection and adversarial robustness. Since GMMC is inspired largely by JEM Grathwohl et al. (2020a), for a fair comparison, our experiments closely follow the settings provided in the source code of JEM². Due to page limit, details of the experimental setup are relegated to Appendix B. All our experiments are performed with PyTorch on Nvidia RTX GPUs.

4.1 HYBRID MODELING

We train GMMC on three benchmark datasets: CIFAR10, CIFAR100 Krizhevsky & Hinton (2009) and SVHN Netzer et al. (2011), and compare it to the state-of-the-art hybrid models, as well as standalone generative and discriminative models. Following the settings of JEM, we use the Wide-ResNet Zagoruyko & Komodakis (2016) as the backbone CNN model for JEM and GMMC. To evaluate the quality of generated images, we adopt Inception Score (IS) Salimans et al. (2016) and Frechet Inception Distance (FID) Heusel et al. (2017). The results on CIFAR10, CIFAR100 and SVHN are shown in Table 1 and Table 2, respectively. It can be observed that GMMC outperforms the state-of-the-art hybrid models in terms of accuracy (94.08%) and FID score (37.0), while being slightly worse in IS score. Since no IS and FID scores are commonly reported on SVHN and CIFAR100, we present the classification accuracies and generated samples on these two benchmarks. Our GMMC models achieve 97.2% and 73.9% accuracy on SVHN and CIFAR100, respectively, outperforming the softmax classifier and JEM by notable margins. Example images generated by GMMC for CIFAR10 are shown in Fig. 3. Additional GMMC generated images for CIFAR100 and SVHN can be found in Appendix F.

Table 1: Hybrid Modeling Results on CIFAR10.

Class	Model	Acc % \uparrow	IS \uparrow	FID \downarrow
Hybrid	Residual Flow	70.3	3.60	46.4
	Glow	67.6	3.92	48.9
	IGEBM	49.1	8.30	37.9
	JEM	92.9	8.76	38.4
	GMMC (Ours)	94.08	7.24	37.0
Disc.	WRN w/ BN	95.8	N/A	N/A
	WRN w/o BN	93.6	N/A	N/A
	GMMC (Dis)	94.3	N/A	N/A
Gen.	SNGAN	N/A	8.59	25.5
	NCSN	N/A	8.91	25.3

4.2 CALIBRATION

While modern deep models have grown more accurate in the past few years, recent researches have shown that their predictions could be over-confident Guo et al. (2017). Outputting an incorrect but confident decision can have catastrophic consequences. Hence, calibration of uncertainty for DNNs is a critical research topic. Here, the confidence is defined as $\max_y p(y|\mathbf{x})$ which is used to decide when to output a prediction. A well-calibrated, but less accurate model can be considerably more useful than a more accurate but less-calibrated model.

²<https://github.com/wgrathwohl/JEM>



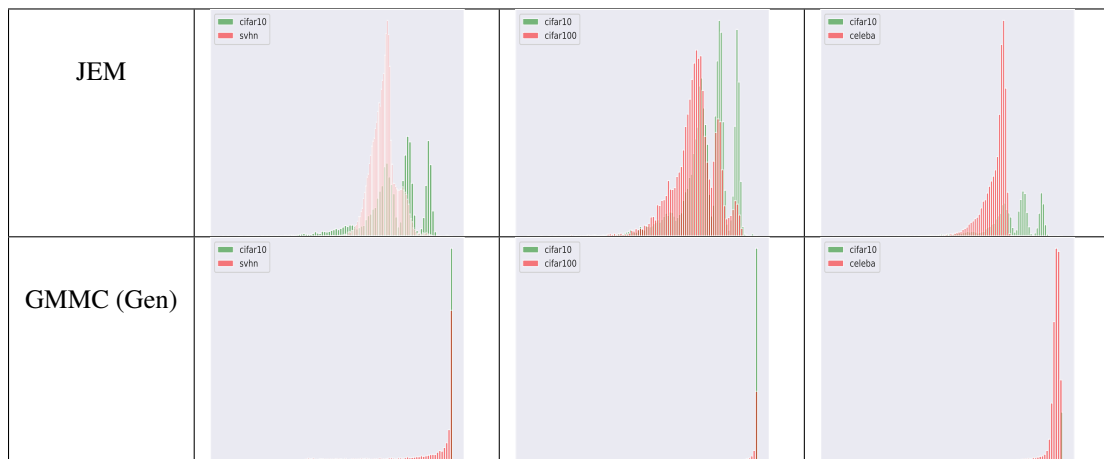
Figure 3: Generated CIFAR10 Samples.

Table 2: Test Accuracy (%) on SVHN and CIFAR100.

Model	SVHN	CIFAR100
Softmax	96.6	72.6
JEM	96.7	72.2
GMMC (Dis)	97.1	75.4
GMMC (Gen)	97.2	73.9

We train GMMC on the CIFAR10 dataset, and compare its Expected Calibration Error (ECE) score Guo et al. (2017) to that of the standard softmax classifier and JEM. Results are shown in Fig. 4 with additional results on SVHN and CIFAR100 provided in Appendix D.1. We find that the model trained by GMMC (Gen) achieves a much smaller ECE (1.33% vs. 4.18%), demonstrating GMMC’s predictions are better calibrated than the competing methods.

4.3 OUT-OF-DISTRIBUTION DETECTION


 Table 3: Histograms of $\log_{\theta} p(\mathbf{x})$ for OOD detection. Green corresponds to in-distribution dataset, while red corresponds to OOD dataset.

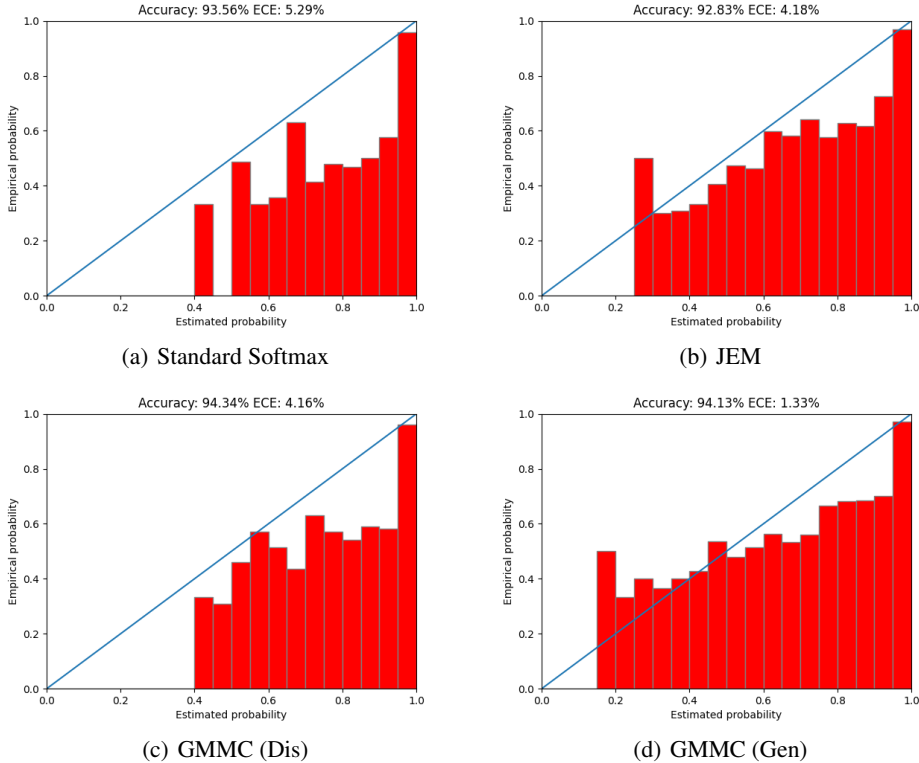


Figure 4: Calibration Results on CIFAR10. The smaller ECE is, the better.

The OOD detection is a binary classification problem, which outputs a score $s_{\theta}(\mathbf{x}) \in \mathbb{R}$ for a given query \mathbf{x} . The model should be able to assign lower scores to OOD examples than to in-distribution examples, such that it can be used to distinguish two sets of examples. Following the settings of JEM Grathwohl et al. (2020a), we use the Area Under the Receiver-Operating Curve (AUROC) Hendrycks & Gimpel (2016) to evaluate the performance of OOD detection. In our experiments, three score functions are considered: the input density $p_{\theta}(\mathbf{x})$ Nalisnick et al. (2018), the predictive distribution $p_{\theta}(y|\mathbf{x})$ Hendrycks & Gimpel (2016), and the approximate mass $\|\frac{\partial \log p_{\theta}(\mathbf{x})}{\partial \mathbf{x}}\|$ Grathwohl et al. (2020a).

Input Density A natural choice of $s_{\theta}(\mathbf{x})$ is the input density $p_{\theta}(\mathbf{x})$. For OOD detection, intuitively we consider examples with low $p(\mathbf{x})$ to be OOD. Quantitative results can be found in Table 4 (top). The corresponding distributions of scores are visualized in Fig. 3. The GMMC model assigns higher likelihoods to in-distribution data than to the OOD data, outperforming all the other models by a significant margin.

Approximate Mass Recent work of Nalisnick et al. (2019) has found that likelihood may not be enough for OOD detection in high-dimensional space. Real samples from a distribution form the area of high probability *mass*. But a point may have a high density while the surrounding area has a very low density, which indicates the density can change rapidly around it and that point is likely not a sample from the real data distribution. Thus, the norm of gradient of the log-density will be large compared to examples in the area *mass*. Based on this reasoning, Grathwohl et al. propose a new OOD score: $\theta(\mathbf{x}) = -\|\frac{\partial \log p_{\theta}(\mathbf{x})}{\partial \mathbf{x}}\|_2$.

Adopting this score function, we find that our model still outperforms the other competing methods (JEM and IGEBM), as shown in Table 4 (bottom).

Predictive Distribution Another useful OOD score is the maximum probability from a classifier’s predictive distribution: $s_{\theta}(\mathbf{x}) = \max_y p_{\theta}(y|\mathbf{x})$. Hence, OOD performance using this score is

Table 4: OOD Detection Results. Models are trained on CIFAR10. Values are AUROC.

$s_{\theta}(\mathbf{x})$	Model	SVHN	Interp	CIFAR100	CelebA
$\log p_{\theta}(\mathbf{x})$	Unconditional Glow	.05	.51	.55	.57
	Class-Conditional Glow	.07	.45	.51	.53
	IGEBM	.63	.70	.50	.70
	JEM	.67	.65	.67	.75
	GMMC (Gen)	.87	.75	.84	.90
$\max_y p_{\theta}(y \mathbf{x})$	Wide-ResNet	.93	.77	.85	.62
	Class-Conditional Glow	.64	.61	.65	.54
	IGEBM	.43	.69	.54	.69
	JEM	.89	.75	.87	.79
	GMMC (Gen)	.84	.72	.81	.31
$\ \frac{\partial \log p_{\theta}(\mathbf{x})}{\partial \mathbf{x}}\ $	Unconditional Glow	.95	.27	.46	.29
	Class-Conditional Glow	.47	.01	.52	.59
	IGEBM	.84	.65	.55	.66
	JEM	.83	.78	.82	.79
	GMMC (Gen)	.88	.79	.85	.87

highly correlated with a model’s classification accuracy. The results can be found in Table 4 (middle). Interestingly, with this score function, there is no clear winner over four different benchmarks consistently, while GMMC performs similarly to JEM in most of the cases.

In summary, among three different OOD score functions, GMMC outperforms all the competing methods by a significant margin with two of them, while being largely on par with another score function. The superior performance of GMMC on OOD is likely due to its *explicit* generative modeling of $p_{\theta}(\mathbf{x}, y)$, which enables exact evaluation of $p_{\theta}(\mathbf{x})$, while other methods cannot.

4.4 ROBUSTNESS

DNNs have demonstrated remarkable success in solving complex prediction tasks. However, recent works Szegedy et al. (2014); Goodfellow et al. (2015); Kurakin et al. (2017) have shown that they are particularly vulnerable to adversarial examples, which are in the form of small perturbations to inputs but can lead DNNs to predict incorrect outputs. Adversarial examples are commonly generated through an iterative optimization procedure, which resembles the iterative sampling procedure of SGLD in Eq. 3. GMMC further utilizes sampled data along with real data for model training (see Eq. 6). This again shares some similarity with adversarial training Goodfellow et al. (2015), which is so far the most effective method to defend adversarial attacks. In this section, we show that GMMC achieves considerable robustness compared to other methods thanks to the MMC modeling Pang et al. (2020) and its generative training.

Table 5: Results under L_{∞} PGD attack with iteration=40. All models are trained on CIFAR10.

Model	Clean (%)	PGD-40	PGD-40	PGD-40	PGD-40
		$\epsilon = 4/255$	$\epsilon = 8/255$	$\epsilon = 16/255$	$\epsilon = 32/255$
Softmax	93.56	19.05	4.95	0.57	0.06
JEM	92.83	34.39	21.23	5.82	0.50
GMMC (Dis)	94.34	44.83	42.22	41.76	38.69
GMMC (Gen)	94.13	56.29	56.27	56.13	55.02

PGD Attack We run the white-box PGD attack Madry et al. (2018) on the models trained by standard softmax, JEM and GMMC. We use the same number of steps (40) with different ϵ as the settings of JEM for PGD. Table 5 provides the test accuracies of different methods. It can be observed that GMMC achieves much higher accuracies than standard softmax and JEM under all

different attack strengths. The superior defense performance of GMMC (Dis) over JEM mainly attributes to the MMC modeling of Pang et al. (2020), while GMMC (Gen) further improves its robustness over GMMC (Dis) due to the generative training.

C&W Attack Pang et al. (2018) reveals that when applying the C&W attack Carlini & Wagner (2017) on their trained networks some adversarial noises have clearly interpretable semantic meanings to the original input images. Tsipras et al. (2018) also discovers that the loss gradient of adversarially trained robust model aligns well with human perception. Interestingly, we also observe similar phenomenon from our GMMC model. Fig. 5 shows some examples of adversarial noises generated from the GMMC (Gen) model under the C&W attack, where the noises are calculated as $(x_{adv} - x)/2$ to keep the pixel values in the range of $[-0.5, 0.5]$. We observe around 5% of adversarial noises have clearly interpretable semantic meanings to their original images. These interpretable adversarial noises indicate that GMMC (Gen) can learn robust features such that the adversarial examples found by the C&W attack have to weaken the features of the original images as a whole, rather than generating salt-and-pepper like perturbations as for the networks of lower robustness.

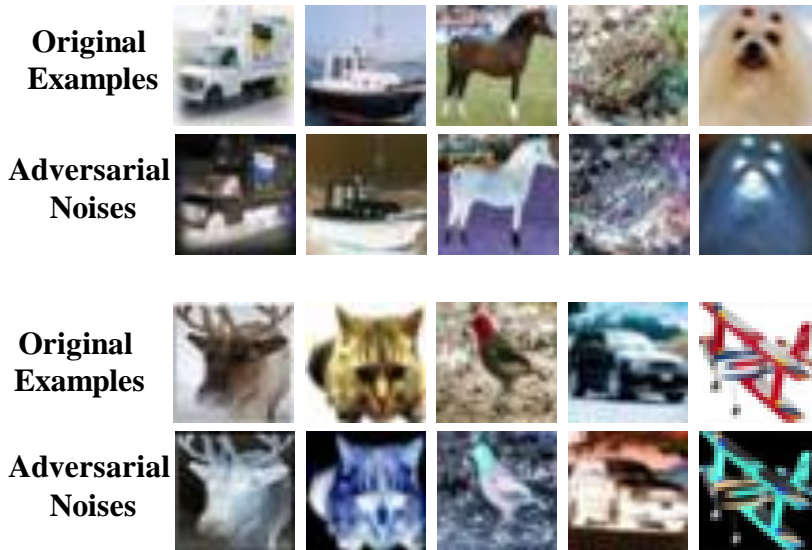


Figure 5: Example adversarial noises generated from the GMMC (Gen) model under C&W attack on CIFAR10.

To have a quantitative measure of model robustness under C&W attack, we apply the C&W attack to the models trained by the standard softmax, JEM and GMMC. In terms of classification accuracy, all of them achieve almost 100% error rate under the C&W attack. However, as shown in Table 6, the adversarial noises to attack the GMMC (Gen) model have a much larger L_2 norm than that of the adversarial noises for other models. This shows that to attack the GMMC (Gen) model, the C&W attack has to add much stronger noises in order to successfully evade the network. In addition, GMMC (Dis) achieves a similar robustness as JEM under the C&W attack, while GMMC (Gen) achieves an improved robustness over GMMC (Dis) likely due to the generative training of GMMC.

Table 6: L_2 norms of adversarial perturbations under C&W attack on CIFAR10.

Model	Untarget, iter=100	Target, iter=1000
Softmax	0.205	0.331
JEM	0.514	0.905
GMMC (Dis)	0.564	0.784
GMMC (Gen)	1.686	1.546

4.5 TRAINING STABILITY

Compared to JEM, GMMC has a well-formulated latent feature distribution, which fits well with the generative process of image synthesis. One advantage we observed from our experiments is that GMMC alleviates most of the instability issues of JEM. Empirically, we find that JEM can train less than 60 epochs before running into numerical issues, while GMMC can run 150 epochs smoothly without any numerical issues in most of our experiments.

4.6 JOINT TRAINING

Finally, we compare the joint training of JEM and GMMC on CIFAR10. The results show that joint training of GMMC is stable, while JEM experiences substantial numerical instability issues. However, the quality of generated images from joint training of GMMC is not as good as generative training of GMMC from scratch. Due to page limit, details of the comparison are relegated to Appendix E.

5 CONCLUSION AND FUTURE WORK

In this paper, we propose GMMC by reinterpreting the max-Mahalanobis classifier Pang et al. (2020) as an EBM. Compared to the standard softmax classifier utilized in JEM, GMMC models the latent feature space explicitly as the max-Mahalanobis distribution, which aligns well with the generative process of image synthesis. We show that GMMC can be trained discriminative, generatively or jointly with reduced complexity and improved stability compared to JEM. Extensive experiments on the benchmark datasets demonstrate that GMMC can achieve state-of-the-art discriminative and generative performances, and improve calibration, out-of-distribution detection and adversarial robustness.

As for future work, we plan to investigate the GMMC models trained by different methods: discriminative vs. generative. We are interested in the differences between the features learned by different methods. We also plan to investigate the joint training of GMMC to improve the quality of generated images further because joint training speeds up the learning of GMMC significantly and can scale up GMMC to large-scale benchmarks, such as ImageNet.

REFERENCES

- Lynton Ardizzone, Radek Mackowiak, Carsten Rother, and Ullrich Köthe. Training normalizing flows with the information bottleneck for competitive generative classification. In *Neural Information Processing Systems (NeurIPS)*, 2020.
- Jens Behrmann, Will Grathwohl, Ricky TQ Chen, David Duvenaud, and Jörn-Henrik Jacobsen. Invertible residual networks. *arXiv preprint arXiv:1811.00995*, 2018.
- Andrew Brock, Jeff Donahue, and Karen Simonyan. Large scale GAN training for high fidelity natural image synthesis. In *International Conference on Learning Representations (ICLR)*, 2019.
- Nicholas Carlini and David Wagner. Towards evaluating the robustness of neural networks. In *IEEE Symposium on Security and Privacy (S&P)*, 2017.
- Olivier Chapelle, Bernhard Scholkopf, and Alexander Zien. Semi-supervised learning. *IEEE Transactions on Neural Networks*, 2009.
- Ricky TQ Chen, Jens Behrmann, David Duvenaud, and Jörn-Henrik Jacobsen. Residual flows for invertible generative modeling. *arXiv preprint arXiv:1906.02735*, 2019.
- Arthur P Dempster, Nan M Laird, and Donald B Rubin. Maximum likelihood from incomplete data via the em algorithm. *Journal of the Royal Statistical Society: Series B (Methodological)*, 39(1): 1–22, 1977.
- Yilun Du and Igor Mordatch. Implicit generation and generalization in energy-based models. *arXiv preprint arXiv:1903.08689*, 2019.

- Ruiqi Gao, Erik Nijkamp, Diederik P. Kingma, Zhen Xu, Andrew M. Dai, and Ying Nian Wu. Flow contrastive estimation of energy-based models. In *IEEE/CVF Conference on Computer Vision and Pattern Recognition (CVPR)*, 2020.
- Ian Goodfellow, Jonathon Shlens, and Christian Szegedy. Explaining and harnessing adversarial examples. In *International Conference on Learning Representations (ICLR)*, 2015.
- Will Grathwohl, Kuan-Chieh Wang, Joern-Henrik Jacobsen, David Duvenaud, Mohammad Norouzi, and Kevin Swersky. Your classifier is secretly an energy based model and you should treat it like one. In *International Conference on Learning Representations (ICLR)*, 2020a.
- Will Grathwohl, Kuan-Chieh Wang, Joern-Henrik Jacobsen, David Duvenaud, and Richard Zemel. Learning the stein discrepancy for training and evaluating energy-based models without sampling. In *Proceedings of the 37th International Conference on Machine Learning (ICML)*, 2020b.
- Chuan Guo, Geoff Pleiss, Yu Sun, and Kilian Q Weinberger. On calibration of modern neural networks. In *Proceedings of the 34th International Conference on Machine Learning-Volume 70*, pp. 1321–1330. JMLR. org, 2017.
- Kaiming He, Xiangyu Zhang, Shaoqing Ren, and Jian Sun. Deep residual learning for image recognition. In *IEEE Conference on Computer Vision and Pattern Recognition (CVPR)*, 2016.
- Dan Hendrycks and Kevin Gimpel. A baseline for detecting misclassified and out-of-distribution examples in neural networks. In *International Conference on Learning Representations (ICLR)*, 2016.
- Martin Heusel, Hubert Ramsauer, Thomas Unterthiner, Bernhard Nessler, and Sepp Hochreiter. Gans trained by a two time-scale update rule converge to a local nash equilibrium. In *Advances in Neural Information Processing Systems*, pp. 6626–6637, 2017.
- Geoffrey E Hinton. Training products of experts by minimizing contrastive divergence. *Neural computation*, 14(8):1771–1800, 2002.
- Diederik Kingma and Jimmy Ba. Adam: A method for stochastic optimization. In *International Conference on Learning Representations (ICLR)*, 2015.
- Alex Krizhevsky and Geoffrey Hinton. Learning multiple layers of features from tiny images. Technical report, Citeseer, 2009.
- Alexey Kurakin, Ian Goodfellow, and Samy Bengio. Adversarial machine learning at scale. In *International Conference on Learning Representations (ICLR)*, 2017.
- Yann LeCun, Sumit Chopra, Raia Hadsell, M Ranzato, and F Huang. A tutorial on energy-based learning. *Predicting structured data*, 1(0), 2006.
- Laurens van der Maaten and Geoffrey Hinton. Visualizing data using t-sne. *Journal of Machine Learning Research (JMLR)*, 9(Nov):2579–2605, 2008.
- Aleksander Madry, Aleksandar Makelov, Ludwig Schmidt, Dimitris Tsipras, and Adrian Vladu. Towards deep learning models resistant to adversarial attacks. In *International Conference on Learning Representations (ICLR)*, 2018.
- Eric Nalisnick, Akihiro Matsukawa, Yee Whye Teh, Dilan Gorur, and Balaji Lakshminarayanan. Do deep generative models know what they don’t know? *arXiv preprint arXiv:1810.09136*, 2018.
- Eric Nalisnick, Akihiro Matsukawa, Yee Whye Teh, and Balaji Lakshminarayanan. Detecting out-of-distribution inputs to deep generative models using a test for typicality. *arXiv preprint arXiv:1906.02994*, 2019.
- Yuval Netzer, Tao Wang, Adam Coates, Alessandro Bissacco, Bo Wu, and Ng Andrew Y. Reading digits in natural images with unsupervised feature learning. 2011.
- Erik Nijkamp, Mitch Hill, Tian Han, Song-Chun Zhu, and Ying Nian Wu. On the anatomy of mcmc-based maximum likelihood learning of energy-based models. *arXiv preprint arXiv:1903.12370*, 2019a.

- Erik Nijkamp, Song-Chun Zhu, and Ying Nian Wu. On learning non-convergent short-run mcmc toward energy-based model. *arXiv preprint arXiv:1904.09770*, 2019b.
- Tianyu Pang, Chao Du, and Jun Zhu. Max-mahalanobis linear discriminant analysis networks. In *International Conference on Machine Learning (ICML)*, 2018.
- Tianyu Pang, Kun Xu, Yinpeng Dong, Chao Du, Ning Chen, and Jun Zhu. Rethinking softmax cross-entropy loss for adversarial robustness. In *International Conference on Learning Representations (ICLR)*, 2020.
- Herbert Robbins and Sutton Monro. A stochastic approximation method. *The Annals of Mathematical Statistics*, pp. 400–407, 1951.
- Tim Salimans, Ian Goodfellow, Wojciech Zaremba, Vicki Cheung, Alec Radford, and Xi Chen. Improved techniques for training gans. In *Advances in neural information processing systems (NeurIPS)*, 2016.
- Shibani Santurkar, Andrew Ilyas, Dimitris Tsipras, Logan Engstrom, Brandon Tran, and Aleksander Madry. Image synthesis with a single (robust) classifier. In *Advances in Neural Information Processing Systems*, 2019.
- Christian Szegedy, Wojciech Zaremba, Ilya Sutskever, Joan Bruna, Dumitru Erhan, Ian Goodfellow, and Rob Fergus. Intriguing properties of neural networks. In *International Conference on Learning Representations (ICLR)*, 2014.
- Dimitris Tsipras, Shibani Santurkar, Logan Engstrom, Alexander Turner, and Aleksander Madry. Robustness may be at odds with accuracy. *arXiv preprint arXiv:1805.12152*, 2018.
- Arash Vahdat and Jan Kautz. NVAE: A deep hierarchical variational autoencoder. In *Neural Information Processing Systems (NeurIPS)*, 2020.
- Weitao Wan, Yuanyi Zhong, Tianpeng Li, and Jiansheng Chen. Rethinking feature distribution for loss functions in image classification. In *Proceedings of the IEEE Conference on Computer Vision and Pattern Recognition (CVPR)*, pp. 9117–9126, 2018.
- Max Welling and Yee W Teh. Bayesian learning via stochastic gradient langevin dynamics. In *Proceedings of the 28th international conference on machine learning (ICML-11)*, pp. 681–688, 2011.
- Jianwen Xie, Yang Lu, Song-Chun Zhu, and Yingnian Wu. A theory of generative convnet. In *International Conference on Machine Learning*, pp. 2635–2644, 2016.
- Sergey Zagoruyko and Nikos Komodakis. Wide residual networks. In *The British Machine Vision Conference (BMVC)*, 2016.
- Stephen Zhao, Jorn-Henrik Jacobsen, and Will Grathwohl. Joint energy-based models for semi-supervised classification. In *ICML 2020 Workshop on Uncertainty and Robustness in Deep Learning*, 2020.

A IMAGE CLASSIFICATION BENCHMARKS

The three image classification benchmarks used in our experiments are described below:

1. CIFAR10 Krizhevsky & Hinton (2009) contains 60,000 RGB images of size 32×32 from 10 classes, in which 50,000 images are for training and 10,000 images are for test.
2. CIFAR100 Krizhevsky & Hinton (2009) also contains 60,000 RGB images of size 32×32 , except that it contains 100 classes with 500 training images and 100 test images per class.
3. SVHN Netzer et al. (2011) is a street view house number dataset containing 73,257 training images and 26,032 test images classified into 10 classes representing digits. Each image may contain multiple real-world house number digits, and the task is to classify the center-most digit.

B EXPERIMENTAL DETAILS

Following JEM Grathwohl et al. (2020a), all our experiments are based on the Wide-ResNet architecture Zagoruyko & Komodakis (2016). To ensure a fair comparison, we follow the same configurations of JEM by removing batch normalization and dropout from the network. We use ADAM optimizer Kingma & Ba (2015) with the initial learning rate of 0.0001 and the decay rate of 0.3, and train all our models for 150 epochs. For CIFAR10 and SVHN, we reduce the learning rate at epoch [30, 50, 80], while for CIFAR100 we reduce the learning rate much later at epoch [120, 140]. The hyperparameters of our generative training of GMMC are listed in Table 7. Compared to the configurations of IGEBM Du & Mordatch (2019) and JEM, we use a 10x larger buffer size and set the reinitialization frequency to 2.5%. We note that with these settings GMMC generates images of higher quality. Comparing the two sampling approaches: Staged Sampling and Noise Injected Sampling, we find that their performances are very similar. Therefore, only the performances of Staged Sampling are provided.

Table 7: Hyperparameters for generative training of GMMC

Variable	Value
Balance factor β	0.5
Number of steps τ	20
Buffer size $ B $	100,000
Reinitialization freq. ρ	2.5%
Step-size α	1.0

C PRE-DESIGNED μ OF MMC

Algorithm 2 describes the construction of a set of means $\mu = \{\mu_y, y = 1, 2, \dots, C\}$ that satisfy the condition of max-Mahalanobis distribution (MMD) Pang et al. (2018). C is the number of classes, d is the dimension of feature vector $\phi(x) \in \mathbb{R}^d$ extracted by CNN, and S is a hyperparameter, which we set to 10 in all our experiments. For more details of MMD, please refer to Pang et al. (2018).

Algorithm 2 GenerateOptMeans(C, d, S) for MMC Pang et al. (2018)

Input: Number of classes C , dimension of feature vector d , and hyperparameter S . ($C \leq d + 1$)

Initialization: Let the C mean vectors be $\mu_1^* = e_1$ and $\mu_i^* = 0_d, i \neq 1$. Here e_1 and 0_d denote the first unit basis vector and the zero vector in \mathbb{R}^d , respectively.

for $i = 2$ **to** C **do**

for $j = 1$ **to** $i - 1$ **do**

$$\mu_i^*(j) = -[1 + \langle \mu_i^*, \mu_j^* \rangle \cdot (C - 1)] / [\mu_j^*(j) \cdot (C - 1)]$$

end for

$$\mu_i^*(i) = \sqrt{1 - \|\mu_i^*\|_2^2}$$

end for

for $k = 1$ **to** C **do**

$$\mu_k^* = S \cdot \mu_k^*$$

end for

Return: The optimal mean vectors $\mu_i^*, i \in [C]$.

D CALIBRATION

Expected Calibration Error (ECE) is a commonly adopted metric to measure the calibration of a model. First, it computes the confidence of the model, $\max_y p(y|x_i)$, for each x_i in the dataset. Then it groups the predictions into equally spaced buckets $\{B_1, B_2, \dots, B_M\}$ based on their confidence scores. For example, if $M = 20$, then B_1 would represent all examples for which the model’s

confidence scores were between 0 and 0.05. Then ECE is calculated as

$$ECE = \sum_{m=1}^M \frac{|B_m|}{n} |\text{acc}(B_m) - \text{conf}(B_m)|, \tag{11}$$

where n is the number of examples in the dataset, $\text{acc}(B_m)$ is the average accuracy of the model on all the examples in B_m and $\text{conf}(B_m)$ is the average confidence on all the examples in B_m . In our experiments, we set $M = 20$. For a perfectly calibrated model, the ECE will be 0 for any M .

D.1 CALIBRATION RESULTS ON CIFAR100 AND SVHN

Figure 6 and Table 8 show the calibration results of GMMC on SVHN and CIFAR100. As we can see, GMMC outperforms the softmax baseline and JEM on SVHN significantly, while JEM works better on CIFAR100.

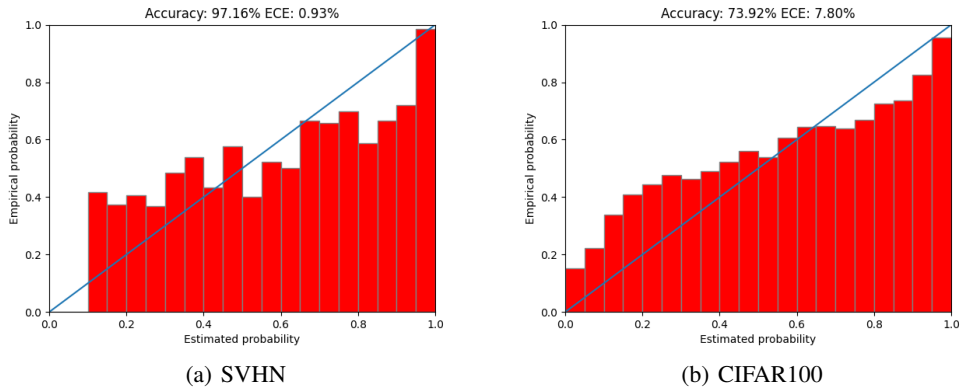


Figure 6: GMMC calibration results on SVHN and CIFAR100.

Table 8: Calibration results on SVHN and CIFAR100.

Model	SVHN	CIFAR100
Softmax	1.91	22.32
JEM	2.08	4.87
GMMC	0.93	7.80

E JOINT TRAINING

Comparing Eq. 4 and Eq. 6 in main text, we note that the gradient of Eq. 4 is just the 2nd term of Eq. 6. Hence, we can use (approach 1) discriminative training to pretrain θ , and then finetune θ by (approach 2) generative training, and this pretraining to finetune strategy would be stable since the first term of Eq. 6 is 0 in expectation. Similar joint training strategy could be applied to train JEM. However, we note that joint training of JEM is extremely unstable.

Figure 7 shows the validation accuracy curves of GMMC trained with discriminative, generative and joint training on CIFAR10. We train each model with 100 epochs, while for the joint training the first 50 epochs are with discriminative training and the rest of 50 epochs are switched to generative training. As we can see, all three models achieve a very similar accuracy of 93.5% in the end. For the joint training, its accuracy drops a little bit around the switching epoch (51th), but finally can catch up to achieve a similar accuracy of 93.5%. Interestingly, we note that the quality of sampled images from joint training, as shown in Figure 8, is not as good as that of generative training from scratch. Nevertheless, this results demonstrate that we can potentially use the joint training to speed

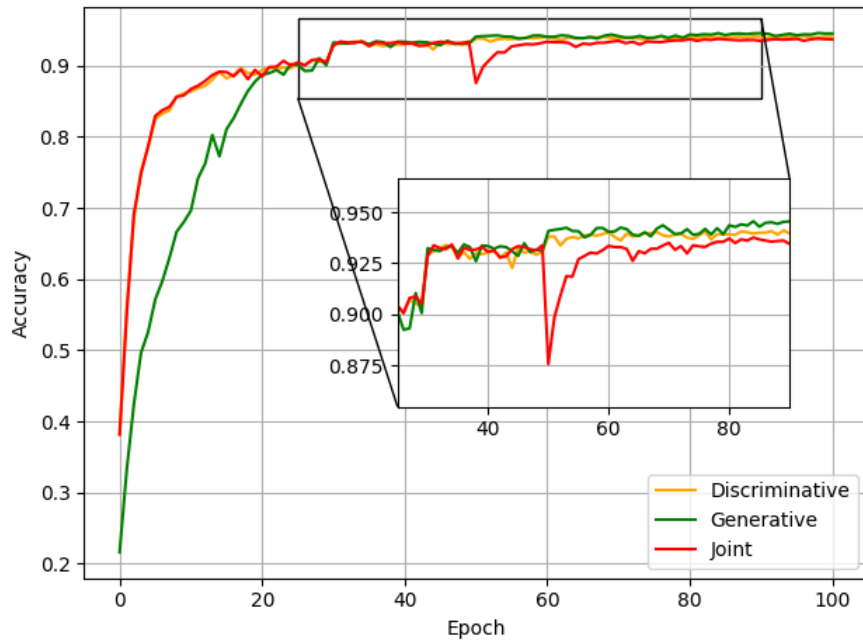


Figure 7: Validation accuracy curves of GMMC trained with discriminative, generative or joint training.

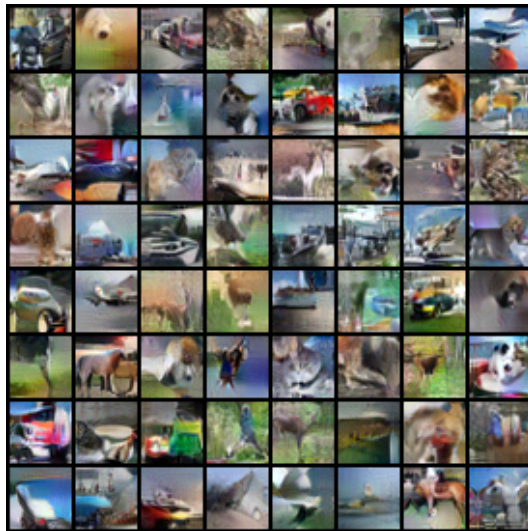


Figure 8: Generated CIFAR10 samples (unconditional) by GMMC with joint training. Compared to the samples from GMMC with generative training, these samples are more blurry.

up the training of GMMC, while generating competitive samples. We leave the improvement of image quality of the joint training of GMMC as our future work.

Similar to the joint training of GMMC, we explore the joint training of JEM, i.e., pretrain the softmax classifier with standard discriminative training and then finetune the softmax classifier with JEM. Table 9 shows the evolution of energy scores of real data and sampled data before and after the switching epoch. Here the energy function is defined as $E_{\theta}(\mathbf{x}) = -\log \sum_y \exp(f_{\theta}(\mathbf{x})[y])$ according to JEM. As can be seen, the energy scores on real data and sampled data are quickly exploded within a few iterations, demonstrating the instability of joint training of JEM. We also use different τ s, the number of SGLD steps, to stabilize JEM but with no success.

Table 9: The energy scores of real data and sampled data after switching from discriminative training to JEM on CIFAR10.

Iteration	Real Data			Sampled Data		
	$\tau = 20$	$\tau = 50$	$\tau = 100$	$\tau = 20$	$\tau = 50$	$\tau = 100$
Before transfer	-22.4	-21.2	-21.6	N/A		
1	-21.5	-19.3	-20.7	-2752	-7369	-13412
2	-9.7	-7.6	-8.5	-67	-243	-556
3	-5.4	-3.9	-3.7	-4	-86	-449
4	-3.2	-2.2	-0.8	294	695	1711
5	-15.4	10.5	13.9	4309	3182	6364
6	524	693	810	1.04e+7	6.34e+6	1.01e+7
7	18676	18250	23021	3.11e+9	3.01e+9	5.15e+9

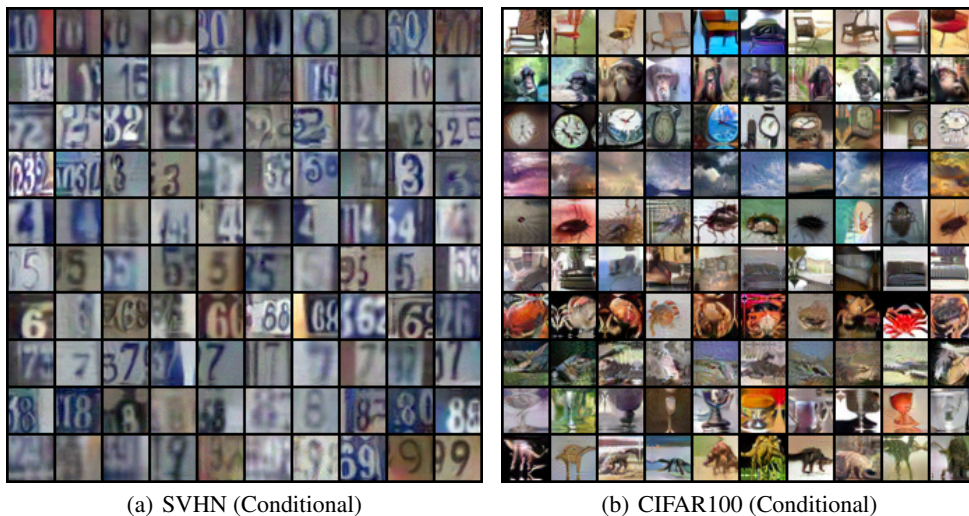


Figure 9: GMMC generated class-conditional samples of SVHN and CIFAR100. Each row corresponds to one class.

F ADDITIONAL GMMC GENERATED SAMPLES

Additional GMMC generated samples of SVHN and CIFAR100 are provided in Figure 9. GMMC generated class-conditional samples of CIFAR10 are provided in Figures 10-19. To evaluate the quality of generated images, we use the same IS and FID code as in IGEBM Du & Mordatch (2019) and JEM Grathwohl et al. (2020a) on the class-conditional samples.

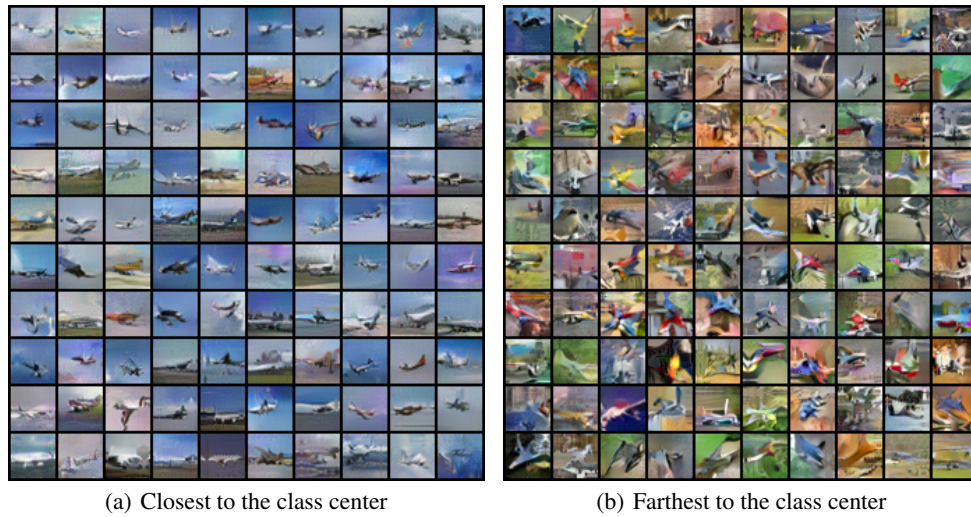


Figure 10: GMMC generated class-conditional samples of **Plane**

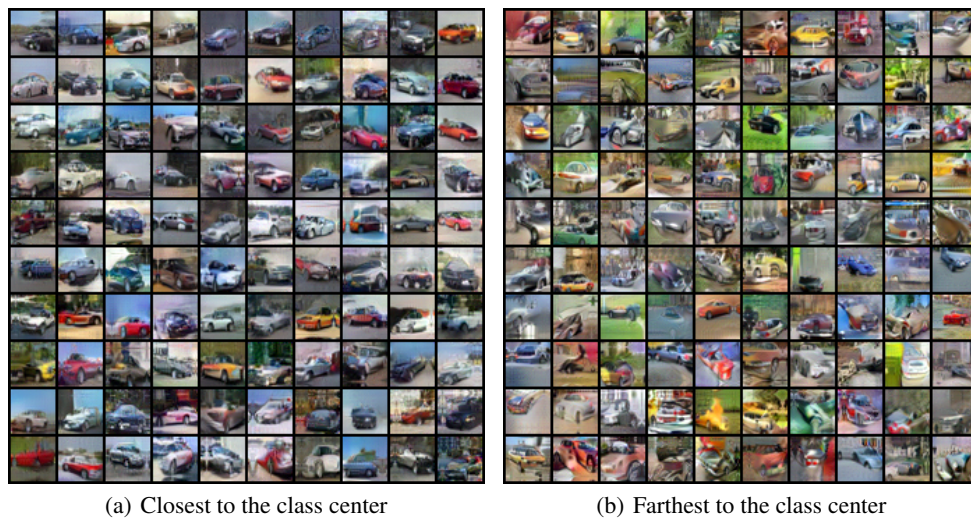


Figure 11: GMMC generated class-conditional samples of **Car**

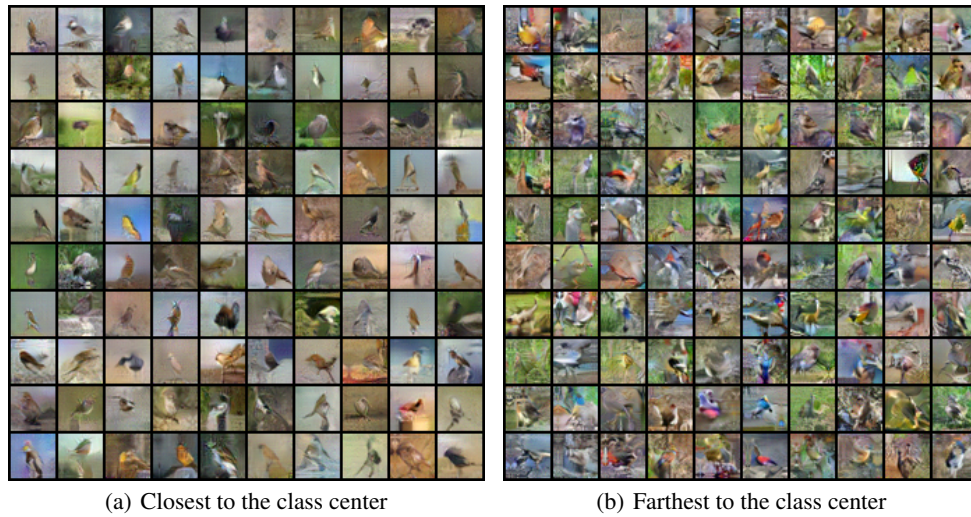


Figure 12: GMMC generated class-conditional samples of **Bird**

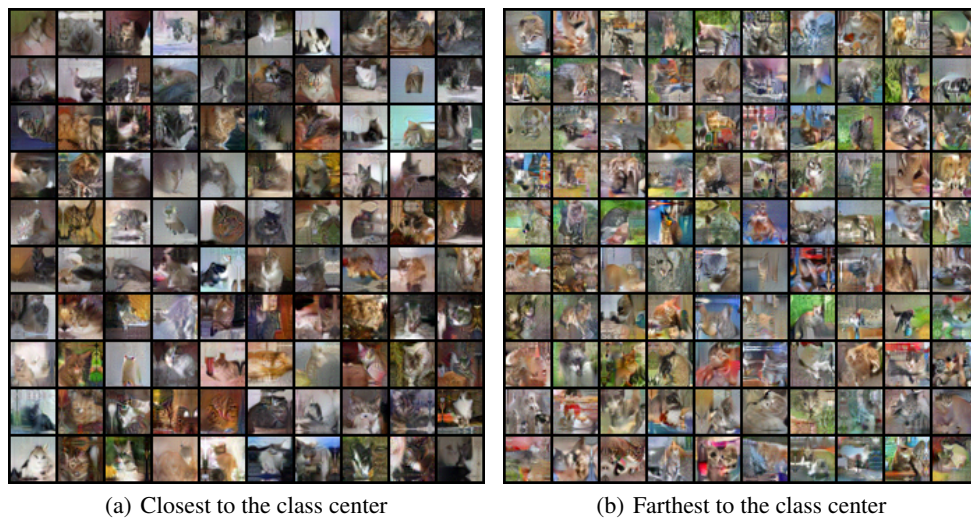


Figure 13: GMMC generated class-conditional samples of **Cat**

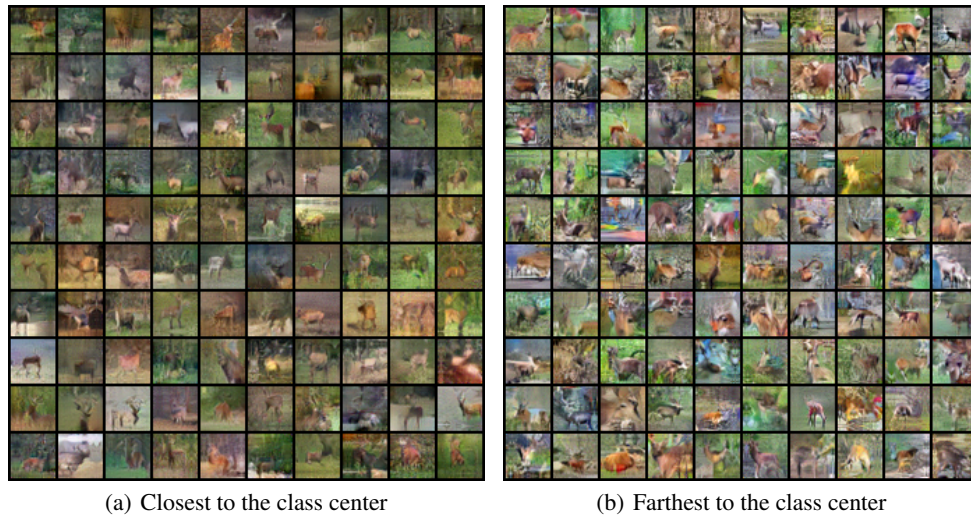


Figure 14: GMMC generated class-conditional samples of **Deer**



Figure 15: GMMC generated class-conditional samples of **Dog**

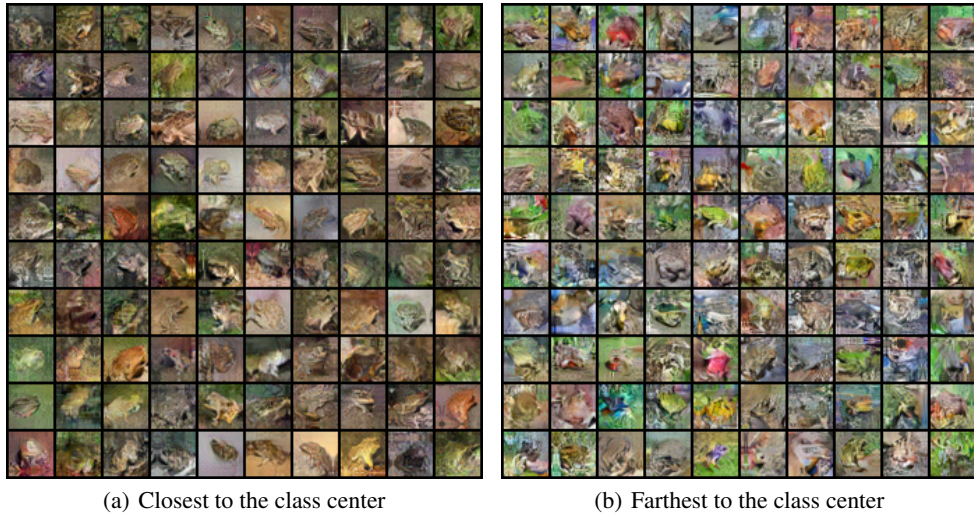


Figure 16: GMMC generated class-conditional samples of **Frog**



Figure 17: GMMC generated class-conditional samples of **Horse**

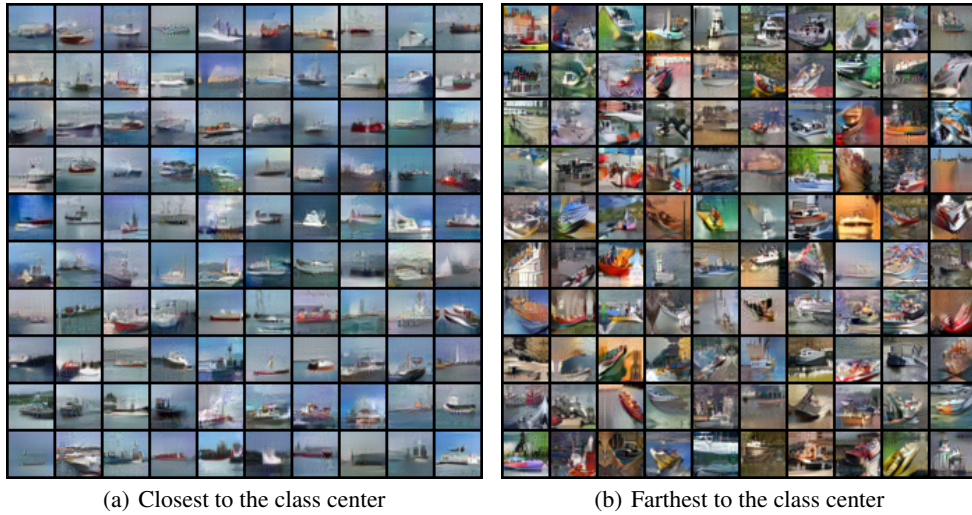


Figure 18: GMMC generated class-conditional samples of **Ship**



Figure 19: GMMC generated class-conditional samples of **Truck**